Chinese Chemical Letters 35 (2024) 108312

Contents lists available at ScienceDirect

Chinese Chemical Letters

journal homepage: www.elsevier.com/locate/cclet

IR780/Gemcitabine-conjugated metal-phenolic network enhanced photodynamic cancer therapy

Songtao Zhou[a,b,c,1], Hao Tian[a,b,1], Jie Yan[a,b], Zhan Zhang[a,b], Guohao Wang[a,b], Xinying Yu[a,b], Wei Sang[a,b], Bei Li[a,b], Greta S.P. Mok[d], Jie Song[c,*], Yunlu Dai[a,b,**]

[a] *Cancer Center and Institute of Translational Medicine, Faculty of Health Sciences, University of Macau, Macau 999078, China*
[b] *MoE Frontiers Science Center for Precision Oncology, University of Macau, Macau 999078, China*
[c] *Institute of Basic Medicine and Cancer (IBMC), Chinese Academy of Sciences, The Cancer Hospital of the University of Chinese Academy of Sciences, Hangzhou 310022, China*
[d] *Biomedical Imaging Laboratory (BIG), Department of Electrical and Computer Engineering, Faculty of Science and Technology, University of Macau, Macau 999078, China*

ARTICLE INFO

Article history:
Received 29 December 2022
Revised 4 March 2023
Accepted 7 March 2023
Available online 12 March 2023

Keywords:
Metal phenolic network
IR780
Photodynamic therapy
Breast cancer
Gemcitabine

ABSTRACT

Photodynamic therapy (PDT) is a clinically approved cancer treatment that uses energy of light to generate active substances that cause damage to the cancer. Photosensitizers are employed to absorb light and generate toxic reactive oxygen species (ROS) to damage biomolecules like DNA. At the same time, some chemotherapy drugs like nucleotide analogues can provide mechanism-guided promotion in the treatment efficacy of PDT. However, the photosensitizer and chemotherapy drugs used in PDT is usually organic molecules, which suffers from bad solubility, fast clearance, and acute toxicity. To achieve targeted treatment, a reasonable delivery system is necessary. Therefore, we reported a metal-phenolic network where IR780 and gemcitabine were coupled chemically to overcome these shortcomings. The enhanced PDT effects can be realized by the promoted cell death both *in vitro* and *in vivo*. Moreover, the synergistic therapy also induced T-cell mediated anti-tumor immune response, which was significant for the inhibition of distant tumor growth. This work expanded the biomedical application of metal-phenolic materials and contribute to the wider application of photodynamic cancer therapy.

Photodynamic therapy (PDT) is a promising therapeutic procedure approved in clinic in the field of oncology [1–3]. Various types of photosensitizers have been developed for PDT, including porphyrins, chlorins, and cyanine derivatives. Followed by irradiation, the light of specific wavelength can activate these photosensitizers to produce reactive oxygen species (ROS), which induce cell apoptosis *via* damaging biology molecules including lipid and DNA. To amplify the PDT efficacy, combination of chemotherapeutic drugs is quite effective. For example, nucleotide analogues have been used clinically for decades to induce DNA damage in cancer cells which provide mechanism-guided promotion in the treatment efficacy of PDT by inhibiting DNA repair and replication [4–10].

However, both photosensitizers and nucleotide analogues suffer from poor solubility and limited biocompatibility which greatly limit their applications. To overcome these limitations and achieve the best therapeutic effect, different strategy such as PEGylation has been developed to improve water solubility and prolong cycle time of hydrophobic drug [11–16]. But only the chemical conjugation cannot achieve targeted delivery to tumor sites. Nowadays, some nano systems have shown great potential in cancer diagnosis and treatment with their advanced tumor accumulation and abundant unique functions [17,18]. Various metal containing nano delivery systems have shown potential for further application [19,20]. Therefore, it is promising to employ nano materials for targeted tumor delivery [21].

Metal-phenol network (MPN) is a newly developed nanovehicle which form stable nanoparticles *via* hydrophobic interaction and phenol-metal coordination [18]. Besides, the pH-responsive coordination also allows the degradation of nanoparticles and release cargoes in acidic tumor microenvironment [22–27]. Our group has been working on expanding application of MPN materials on cancer theragnostics and realized effective suppression for various types of tumors in different therapies [28–40].

In this work, we exploited IR780 as PDT agent [41] that induced significant DNA damages when exposed to laser irradiation. And gemcitabine was introduced to enhance the therapeutic effects of

* Corresponding author.
** Corresponding author at: Cancer Center and Institute of Translational Medicine, Faculty of Health Sciences, University of Macau, Macau 999078, China.
E-mail addresses: sjie@sjtu.edu.cn (J. Song), yldai@um.edu.mo (Y. Dai).
[1] These authors contributed equally to this work.

https://doi.org/10.1016/j.cclet.2023.108312
1001-8417/

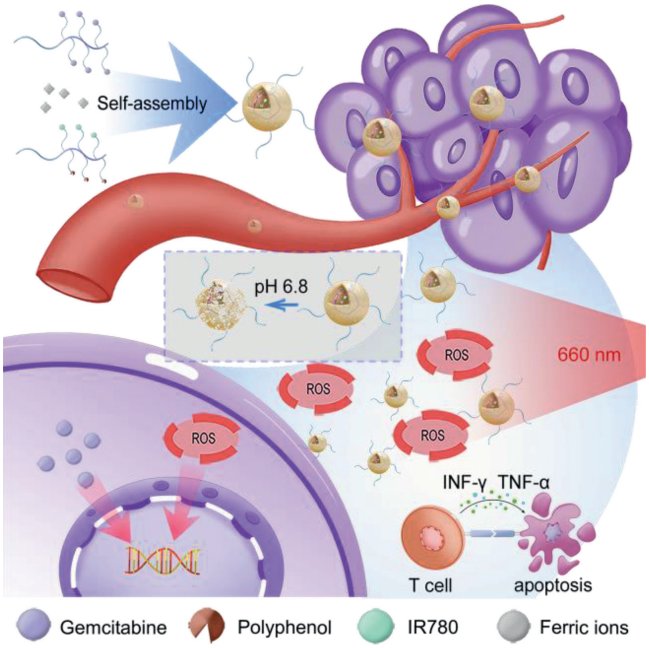

Scheme 1. Schematic illustration about the design of the metal-phenolic network. The IR780 and gemcitabine were PEGylated to form metal phenolic network (MPN) to overcome their inherent defects. And the synergistic therapy enhanced photodynamic therapy by promoting cell apoptosis and facilitating T-cell mediated antitumor immune response.

PDT by inhibiting DNA repair. Both IR780 and gemcitabine were PEGylated into phenolic polymer and form NP in presence of ferric ions (Scheme 1). The experiments *in vitro* and *in vivo* can confirm the enhanced PDT performance. Furthermore, the synergistic therapy also induced anti-tumor immune response, which inhibited the growth of distant tumor [42,43].

Based on our previous work, we designed and synthesized two amphiphilic polymers (PEG-IR780 & PEG-Gem) to overcome these disadvantages of IR780 and gemcitabine [28,44]. The chemical structure and synthesis route has been shown Figs. S1 and S2 (Supporting information), the polyethylene glycol (PEG5000) was chosen as the hydrophilic chain. To synthesize the polymers, the polymers containing free amino groups or *N*-hydroxysuccinimide (NHS) groups at the hydrophobic alkane chain were obtained through reversible addition fragmentation chain transfer (RAFT) reaction. Subsequently, polyphenol, IR780 and gemcitabine were decorated into the polymers, respectively. The final products were characterized and quantified by UV and ^{1}H NMR (Figs. S3-S5 in Supporting information). The number of gemcitabine molecules on PEG-Gem was about 12–13, quantified by analyzing the characteristic peak of gemcitabine at 269 nm (Figs. S3 and S4). The number of IR780 and catechol on PEG-IR780 was about 8 and 6 respectively quantified by ^{1}H NMR (Fig. S5). The conjugation of gemcitabine is reversible in acidic environment according to previous work, endowing it pH-responsive ability (Fig. S6a in Supporting information) [45]. Therefore, we measured the drug release rate of gemcitabine from PEG-Gem in different pH conditions. It increased significantly when pH was reduced from 7.4 to 6.5 (Fig. S6b in Supporting information).

For the preparation of NP, two polymers at the same concentration were added to Fe^{3+} aqueous solution under ultrasonic condition to trigger the rapid assembling of NP *via* hydrophobic interaction and metal-phenolic coordination (Fig. 1A). The size and morphology were determined by DLS and TEM, where the average diameter of particles was 76.7 nm (Figs. 1B and C). The surface charge of the NP was also determined, where the zeta potential of the NP was 14.9 mV (Fig. S7 in Supporting information). Inductively coupled plasma mass spectrometry (ICP-MS) was used to quantify ferric ions in NP, where the mass proportion of Fe^{3+} in NP was 0.68%. To further confirm the stability, we monitored the size of the particles in 7 days and found the particle was quite stable in one week after assembling (Fig. S8 in Supporting information). Furthermore, we found the modified IR780 showed a blue shift in absorption (640 nm) and the fluorescence at about 750 nm (Fig. 1D). Then we evaluated the PDT effect of the NP. 1,3-Diphenylisobenzofuran (DPBF) was a specific ROS probe, which was chosen for the detection of ROS production. the result showed that the nanoparticles could amplify the ROS generation significantly under the 660 nm laser irradiation (Fig. 1E).

Mice breast cancer cell 4T1 was chosen for therapeutic experiments. Firstly, the red fluorescence from IR780 was exploited to

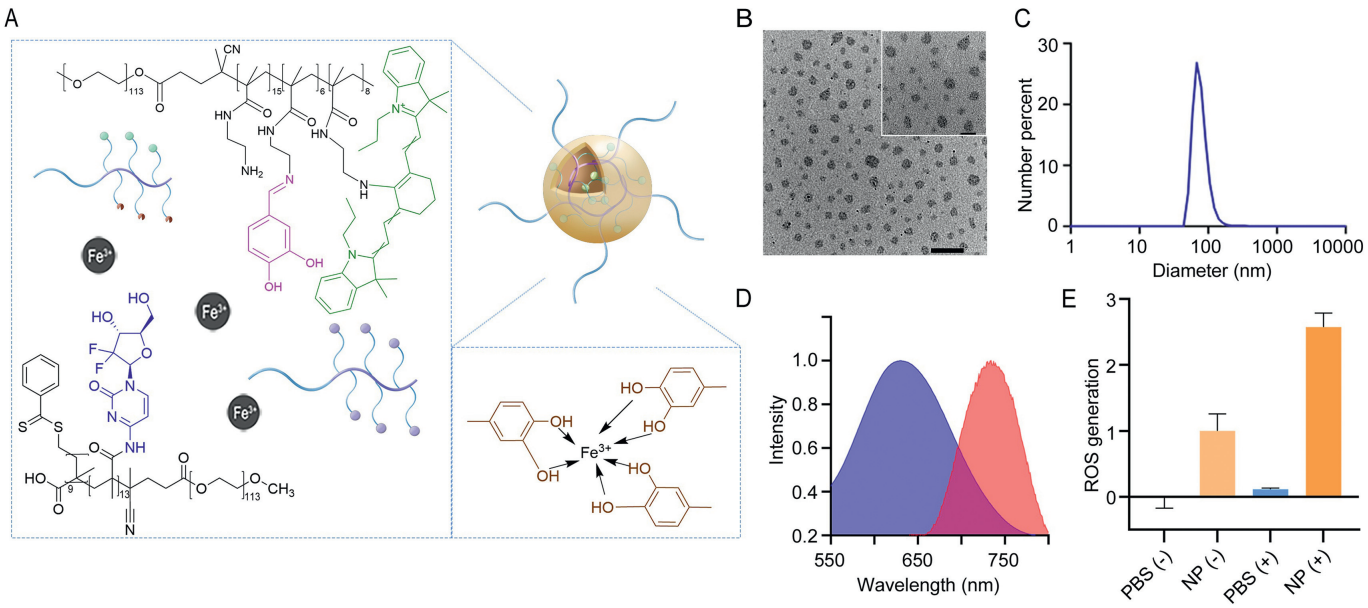

Fig. 1. Design and characterization of NP. (A) Scheme of NP. (B) TEM images of NP. Scale bar: external 500 nm and internal 200 nm. (C) Size distribution of NP determined DLS. (D) Absorption (blue) and emission (red) of NP. (E) ROS generation of the NP under 660 nm laser irradiation. (+): with 660 nm laser, (−): without 660 nm laser, 1 W/cm^2. Data are presented as mean values ± SD ($n = 3$).

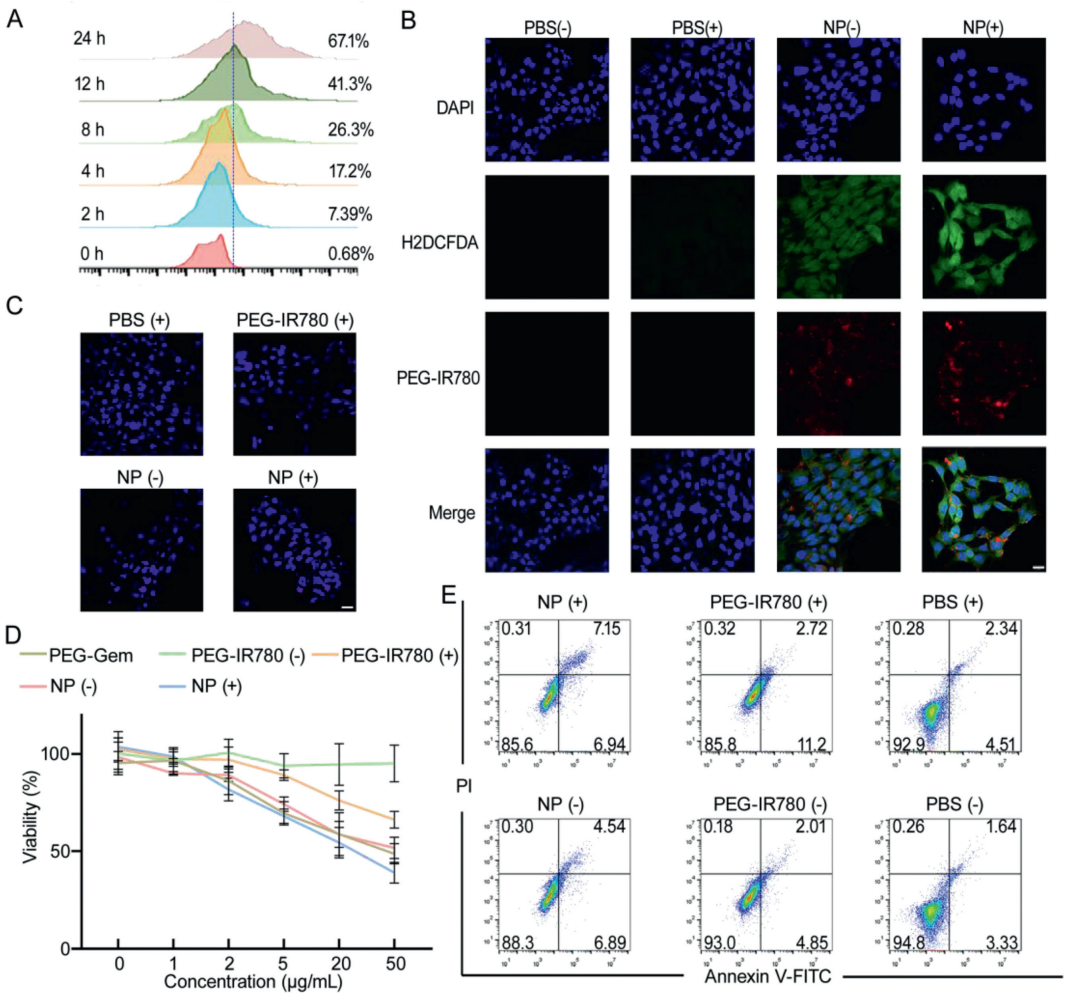

Fig. 2. *In vitro* experiments. (+): with 660 nm laser, (−): without 660 nm laser, 1 W/cm^2. (A) Cell uptake of NP. (B) Confocal microscopy images of ROS production and the distribution of NP (scale bar: 20 μm). (C) DNA damage under different treatments. Red fluorescence represents DNA double strand break while blue fluorescence represents DNA (scale bar: 20 μm). (D) Cytotoxicity of different treatments by MTT assay, the concentration was determined by polymer mass concentration. (E) Apoptosis rate (%) after different treatments staining with Annexin V-FITC and PI. Data are presented as mean values ± SD ($n = 3$).

evaluate the cellular uptake of NP. The change of fluorescence intensity at different time points (0, 2, 4, 8, 12, 24 h) showed the cellular uptake behavior increased over time and it was found that 24 h is enough for most NP being administrated (Fig. 2A). Intracellular ROS production was evaluated by the fluorescence probe H2DCFDA which reacted with singlet oxygen and generated a green fluorophore. Due to the self-fluorescence of PEG-IR780, the intracellular biodistribution of the NP could also been traced by red fluorescence (Fig. 2B). The obvious increase in green fluorescence under irradiation indicated the ROS generation. The co-location of green and red fluorescence also demonstrated the spatiotemporal consistency of the NP and produced ROS. To confirm the amplified DNA damage, antibody against γ-H_2AX was used to detect DNA double strand breaks. Treated with NP and 660 nm laser, a stronger red fluorescence was generated and merged with the blue fluorescence from DAPI to produce a purple signal (Fig. 2C). Methyl thiazolyl tetrazolium (MTT) assay was conducted to evaluate the cytotoxicity of various treatments (Fig. 2D). Compared with laser irradiation or gemcitabine alone, NP combined with laser treatment got the best anti-cancer effects, which demonstrated the synergistic treatment can enhance PDT. Annexin V/PI apoptosis staining was performed to further confirm the enhanced PDT of NP (Fig. 2E). Combining NP and irradiation treatment, total apoptosis ratios obviously increased from 4.99% to 14.09% compare with control group.

Encouraged by the good performance of the NP *in vitro*, further experiments *in vivo* were conducted. All animal studies were approved by the University of Macau Animal Ethics Committee following the standard protocol (UMARE-030–2018). As mentioned before, PEGylation tend to prolong the residence time and facilitate tumor accumulation. The fluorescence from IR780 was used to monitor the biodistribution of NP. In this experiments, 4T1 tumor-bearing mice model was chosen. After the intravenous injection of NP, the *in vivo* fluorescent imaging was conducted at different time points (1, 4, 8, 12, 24 h). Initially, the fluorescence in tumor site increased and then gradually decrease, peaked at 4–8 h (Fig. 3A). And the total fluorescent intensity was quantified (Fig. 3B). Moreover, the fluorescence in tumor site was still remarkable at 24 h. Then the tumors and main organs (heart, liver, spleen, lung, kidney) were collected for *ex vivo* fluorescent imaging. The corresponding quantification results further confirm the high tumor accumulation (Figs. 3C and D).

Then we evaluated the *in vivo* antitumor effects of the NP on bilateral subcutaneous tumor-bearing mice model, and the procedure is shown in Fig. 3E. When the primary tumor volume reached 200 mm^3, all mice were randomly divided into six groups: G1: PBS, G2: PEG-Gem, G3: PEG-IR780 (−), G4: PEG-IR780 (+), G5: NP (−), G6: NP (+), where (+) represents the 660 nm laser treatment at 6 h after injection. To avoid potential photothermal therapy (PTT) effect, we took 30 s intervals for cooling down after every 30 s laser

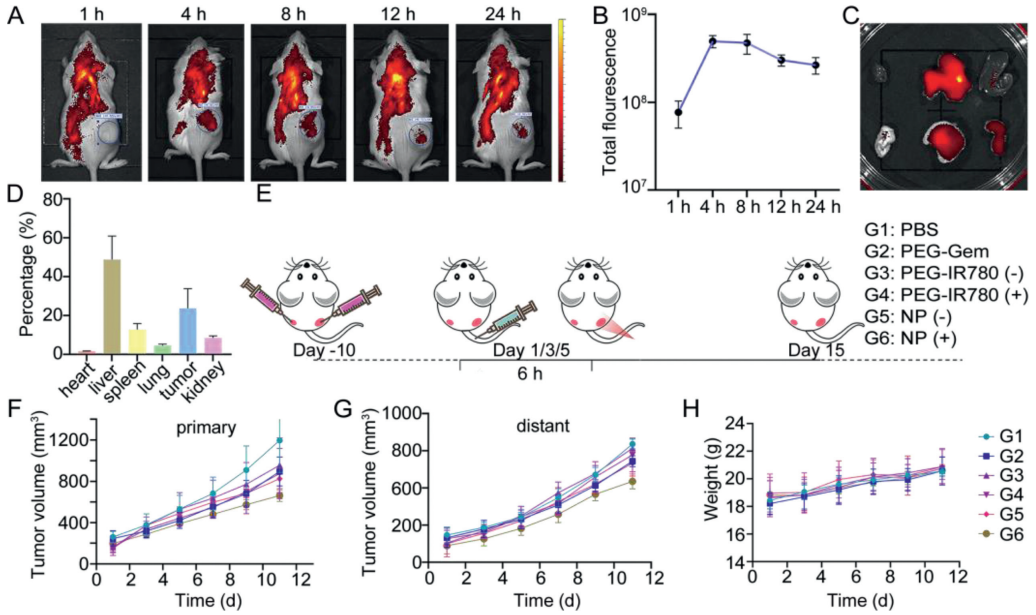

Fig. 3. *In vivo* experiments. (A) *In vivo* fluorescent images at different time points. (B) Quantitative analysis of the total fluorescence in tumor areas ($n = 3$). (C) *Ex vivo* fluorescent images of major organs at 24 h post-injection. (D) Quantitative analysis of *ex vivo* fluorescence at 24 h post-injection. (E) Anti-tumor experiment procedure (dose of drug was quantified by polymer:100 μg/mice). (F) Primary tumor volume. (G) Distant tumor volume. (H) Body weight of mice. G1: PBS, G2: PEG-Gem, G3: PEG-IR780 (−), G4: PEG-IR780 (+), G5: NP (−), G6: NP (+), where (+) represent the 660 nm laser treatment 6 h after injection. Data are presented as mean values ± SD ($n = 4$).

treatment. The volume of tumors and body weight were monitored and recorded every two days until all mice were sacrificed on day 15. The main organs, serum, and tumors were collected for further analysis. Compared with the PBS group, the two polymers, PEG-Gem and PEG-IR780 alone only had a slight tumor suppressing effect (Fig. 3F). And as expected, the NP treated mice supported with irradiation got the best tumor suppression for both primary and distant tumor (Figs. 3F and G), which indicated the effective synergy of NP and PDT. We assume the therapy effects for distant tumor was achieved *via* the immune response.

To evaluate the biomedical safety of the NP, we traced the body weights of mice during treatments, analyzed biochemical parameters of serum, and evaluate the histomorphology changes of major organs of mice *via* H&E staining. The body weight of the mice under different treatment showed no obvious difference (Fig. 3H). After being sacrificed, mice serum was collected and blood biochemical parameters was evaluated (Fig. S9 in Supporting information), including lactate dehydrogenase (LDH), creatine kinase (CK), glutamic oxaloacetic transaminase (GOT), glutamic pyruvic transaminase (GPT), blood urea nitrogen (BUN), and creatinine (CR). Those paraments did not show significant difference among groups that indicate this NP has no obvious side effects on the mice body. H&E staining of major organs demonstrated that the histomorphology of the heart, liver, spleen, lung, and kidney was not affected noticeably (Fig. S10 in Supporting information). 4T1 cells induced tumor is known to be highly migratory, so we also evaluated the lung

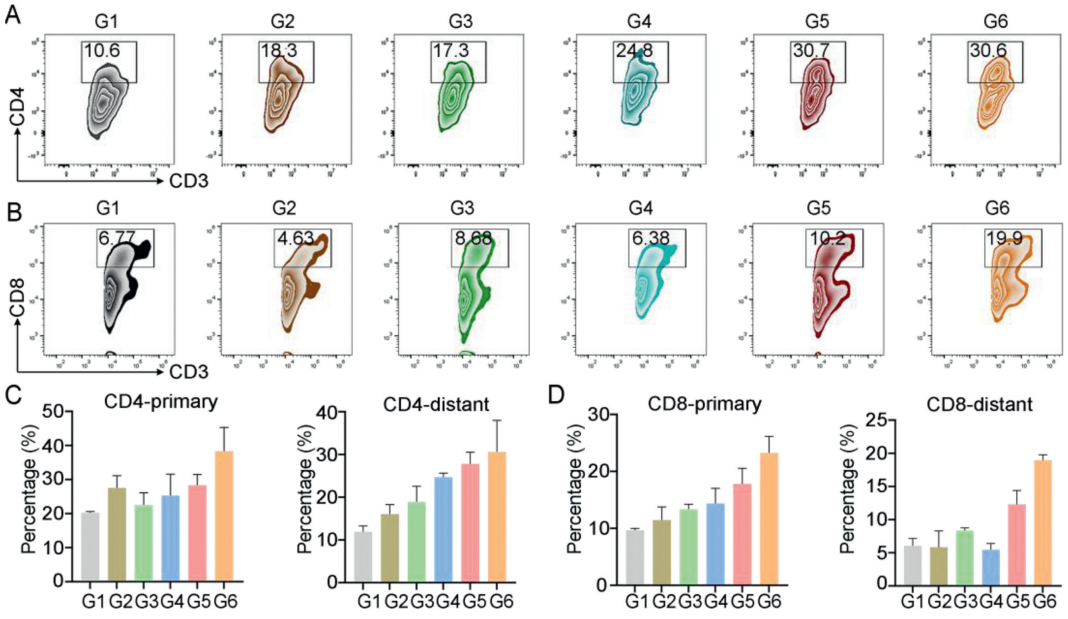

Fig. 4. Immune evocation. Flow cytometric and quantitative analysis of $CD4^+$ T cells (A) and $CD8^+$ T cells (B) in distant tumors. Quantification data of $CD4^+$ T cells (C) and $CD8^+$ T cells (D) in primary and distant tumors. G1: PBS, G2: PEG-Gem, G3: PEG-IR780 (−), G4: PEG-IR780 (+), G5: NP (−), G6: NP (+), where (+) represent the 660 nm laser treatment 6 h after injection. Data were presented as mean values ± SD ($n = 3$).

metastasis to see if this treatment could also suppress tumor migration. Bouin's fixative solution was used to fix the collected lungs after treatments. By observing the metastasis nodules on lung surface (Fig. S11 in Supporting information). We found this treatment can also slow the lung metastasis process.

We hypothesized that the inhibitory effect on distant tumor growth was mainly due to the antitumor immune response. As a representative, we investigated the T cells activation and filtration in tumor. Helper T cells ($CD3^+$ $CD4^+$) and cytotoxic T cells ($CD3^+$ $CD8^+$) in primary and distant tumors was evaluated by flow cytometry. The total percent of $CD4^+$ helper T cells and $CD8^+$ cytotoxic cells in $CD3^+$ cells increased (Figs. 4A and C, Fig. S12 in Supporting information). These improvements could be more obvious in distant tumor where $CD4^+$ cell percent was increase from 10.4% to 30.7% and $CD8^+$ cells also increase from 6.77% to 19.9% (Figs. 4B and D, Fig. S13 in Supporting information). Moreover, relative high level of IFN-γ and TNF-α in tumor may imply an improved immune environment after treatments (Fig. S14 in Supporting information). These results indicate this NP will facilitate the T-cell mediated immune response in tumor.

To make a summary, we decorated IR780 and gemcitabine into phenolic polymer to form NP, which overcome the poor solubility and increase the cycle time of the two hydrophobic drugs. The MPN delivery system also endowed it good tumor accumulation and pH-responsive drug release, which increased the selectivity of the drugs and reduce the toxicity to normal tissues. The DNA was damaged by PDT, and DNA repair and replication was inhibited by gemcitabine thus aggravate the damage and suppressed tumor growth. Furthermore, this NP could also evoke immune response and suppress distant tumor growth. We highlight the advantages of the MPN delivery system and expand its application where chemical conjugation could be used to improve the biocompatibility and effects of hydrophobic drugs. Metal-containing nanodrugs have been widely used in cancer diagnosis and treatment. We combined the advantages of different therapeutic agents with MPN delivery system, which could broaden our acknowledge of nano delivery system for cancer and contribute to the wider application of metal-containing nanodrugs and photodynamic cancer therapy.

Declaration of competing interest

The authors declare that they have no known competing financial interests or personal relationships that could have appeared to influence the work reported in this paper.

Acknowledgments

This work was supported by the National Natural Science Foundation of China (NSFC, Nos. 32171318, 32222090 and 32101069), the Faculty of Health Sciences, University of Macau, the Multi-Year Research Grant (MYRG) of University of Macau (No. MYRG2022–00011-FHS), the Science and Technology Development Fund, Macau SAR (Nos. 0103/2021/A and 0002/2021/AKP), Shenzhen Science and Technology Innovation Commission, Shenzhen-Hong Kong-Macau Science and Technology Plan C (No. SGDX20201103093600004), and Dr. Stanley Ho Medical Development Foundation (No. SHMDF-OIRFS/2022/002) The authors appreciate the assistance and support from the Proteomics, Metabolomics, and Drug Development Core, Animal Research Core, and Biological Imaging and Stem Cell Core in the Faculty of Health Sciences, University of Macau.

Supplementary materials

Supplementary material associated with this article can be found, in the online version, at doi:10.1016/j.cclet.2023.108312.

References

[1] D.E.J.G.J. Dolmans, D. Fukumura, R.K. Jain, Nat. Rev. Cancer 3 (2003) 380–387.
[2] L. Cheng, C. Wang, L. Feng, et al., Chem. Rev. 114 (2014) 10869–10939.
[3] C. Xu, K. Pu, Chem. Soc. Rev. 50 (2021) 1111–1137.
[4] M. Amrutkar, I.P. Gladhaug, Cancers (Basel) 9 (2017) 157.
[5] K. Kattel, G. Mondal, F. Lin, et al., Mol. Pharmaceut. 14 (2017) 1365–1372.
[6] S. Dyawanapelly, A. Kumar, M.K. Chourasia, Crit. Rev. Ther. Drug Carrier Syst. 34 (2017) 63–96.
[7] A. Schaefer, L. Schomacher, G. Barreto, et al., PLoS One 5 (2010) e14060.
[8] A. Wong, R.A. Soo, W.P. Yong, F. Innocenti, Drug Metab. Rev. 41 (2009) 77–88.
[9] E. Mini, S. Nobili, B. Caciagli, et al., Ann. Oncol. 17 (Suppl. 5) (2006) v7–v12.
[10] W. Plunkett, P. Huang, V. Gandhi, Anticancer Drugs 6 (1995) 7–13.
[11] T. Min, H. Ye, P. Zhang, et al., J. Appl. Polym. Sci. 111 (2009) 444–451.
[12] H.K. Choi, M.K. Chun, S.H. Lee, et al., Int. J. Pharm. 341 (2007) 50–57.
[13] C.D. Conover, H. Zhao, C.B. Longley, et al., Bioconjugate Chem. 14 (2003) 661–666.
[14] A.P. Castano, T.N. Demidova, M.R. Hamblin, Photodiagn. Photodyn. Ther. 1 (2004) 279–293.
[15] S. Luo, E. Zhang, Y. Su, et al., Biomaterials 32 (2011) 7127–7138.
[16] K. Kassab, J. Photochem. Photobiol. B: Biol. 68 (2002) 15–22.
[17] L. Zhu, L. Chan, J. Wang, et al., Nano Res. 16 (2023) 5169–5175.
[18] J. Li, H. Luo, X. Zhu, J. Zhao, T. Chen, Chin. Chem. Lett. 33 (2022) 788–792.
[19] M. Chen, X. Huang, J. Lai, et al., Chin. Chem. Lett. 32 (2021) 158–161.
[20] L. Xie, Z. Luo, Z. Zhao, T. Chen, J. Med. Chem. 60 (2017) 202–214.
[21] D. de Melo-Diogo, C. Pais-Silva, D.R. Dias, et al., Adv. Healthc. Mater. 6 (2017) 1700073.
[22] Y. Dai, J. Guo, T. Wang, et al., Adv. Healthc. Mater. 6 (2017) 1700467.
[23] J. Chen, S. Pan, J. Zhou, et al., Adv. Mater. 34 (2022) 2108624.
[24] C.J. Kim, F. Ercole, J. Chen, et al., J. Am. Chem. Soc. 144 (2022) 503–514.
[25] P. Liu, X. Shi, S. Zhong, et al., Biomater. Sci. 9 (2021) 2825–2849.
[26] W. Xie, Z. Guo, L. Zhao, Y. Wei, Theranostics 11 (2021) 6407–6426.
[27] Z. Zhang, L. Xie, Y. Ju, Y. Dai, Small 17 (2021) 2100314.
[28] H. Tian, G. Wang, W. Sang, et al., Nano Today 43 (2022) 101405.
[29] W. Sang, Z. Zhang, G. Wang, et al., Adv. Funct. Mater. 32 (2022) 2113168.
[30] J. Yan, G. Wang, L. Xie, et al., Adv. Mater. 34 (2022) 2105783.
[31] L. Xie, J. Li, G. Wang, et al., J. Am. Chem. Soc. 144 (2022) 787–797.
[32] W. Li, L. Xie, Y. Ju, et al., Nano Res. 15 (2022) 3458–3470.
[33] J. Li, W. Li, L. Xie, et al., Chem. Commun. 57 (2021) 11473–11476.
[34] Z. Zhang, B. Li, L. Xie, et al., ACS Nano 15 (2021) 16934–16945.
[35] G. Wang, L. Xie, B. Li, et al., Nat. Commun. 12 (2021) 5733.
[36] J. Li, L. Xie, B. Li, et al., Adv. Mater. 33 (2021) 2008481.
[37] W. Sang, L. Xie, G. Wang, et al., Adv. Sci. 8 (2021) 2003338.
[38] Z. Zhang, W. Sang, L. Xie, et al., Angew. Chem. Int. Ed. 60 (2021) 1967–1975.
[39] J. Yan, B. Li, P. Yang, et al., Adv. Funct. Mater. 31 (2021) 2104325.
[40] C. Lu, Y. Tian, H. Tian, et al., Sci. China Mater. 66 (2023) 395–406.
[41] C. Zhang, T. Liu, Y. Su, et al., Biomaterials 31 (2010) 6612–6617.
[42] J. Hua, P. Wu, L. Gan, et al., Front. Oncol. 11 (2021) 738323.
[43] F. Anzengruber, P. Avci, L.F. de Freitas, M.R. Hamblin, Photochem. Photobiol. Sci. 14 (2015) 1492–1509.
[44] Z. Ren, S. Sun, R. Sun, et al., Adv. Mater. 32 (2020) 1906024.
[45] M. Vandana, S.K. Sahoo, Biomaterials 31 (2010) 9340–9356.